SI Appendix

Regulation of nuclear epigenome by mitochondrial DNA heteroplasmy

Piotr K Kopinski[1,2,3], Kevin A Janssen[4], Patrick M Schaefer[3], Sophie Trefely[5,6], Caroline E Perry[3], Prasanth Potluri[3], Jesus A Tintos-Hernandez[3], Larry N Singh[3], Kelly R Karch[4], Sydney L Campbell[5], Mary T Doan[6], Helen Jiang[6], Itzhak Nissim[7], Eiko Nakamaru-Ogiso[6], Kathryn E Wellen[5], Nathaniel W Snyder[6], Benjamin A Garcia[4], Douglas C Wallace* [3,8]

1. Howard Hughes Medical Institute, University of Pennsylvania, Philadelphia, PA 19104, USA
2. Perelman School of Medicine, University of Pennsylvania, Philadelphia, PA 19104, USA
3. Center for Mitochondrial and Epigenomic Medicine, Children's Hospital of Philadelphia, Phiadelphia, PA 19104, USA
4. Epigenetics Institute, Department of Biochemistry and Biophysics, Perelman School of Medicine, University of Pennsylvania, Philadelphia, PA, USA.
5. Department of Cancer Biology, Perelman School of Medicine, University of Pennsylvania, Philadelphia, PA 19104, USA
6. Drexel University, A.J. Drexel Autism Institute, 3020 Market Street , Philadelphia Pennsylvania 19104 , USA
7. Department of Biochemistry and Biophysics, University of Pennsylvania Perelman School of Medicine, Philadelphia, PA 19104, USA
8. Department of Pediatrics, Division of Human Genetics, The Children's Hospital of Philadelphia, Perelman School of Medicine, University of Pennsylvania, Philadelphia, PA 19104, USA

Supplementary Figure 1. Effect of mtDNA tRNA$^{Leu(UUR)}$ nt 3243G heteroplasmy on nuclear gene transcription. Whole cell transcriptional profiles determined by RNA-sequencing of mRNA extracted from 0, 20, 30, 60, 70, 90, and 100% m.3243G heteroplasmic cybrid lines plus parental 143B(TK$^-$) ρ^0 cell line, defined by three way principal component analysis. Clusters of cybrid cell lines transcriptional profiles harbor heteroplasmic levels which correspond to those associated with distinct clinical phenotypes, printed in red. Reproduced from ref. 1.

Supplementary Figure 2. Methodology for analysis of heteroplasmy cell lines; Cells with various degrees of heteroplasmy were cultured in parallel for histone and metabolite isolation and quantification. The data was obtained from two different laboratories and correlated using the Spearman method in R software. Associations are presented in color for $p < 0.05$. Positive correlations = blue, negative = red. Darker the color, the stronger the correlation.

Supplementary Figure 3. Effect of mtDNA tRNA$^{Leu(UUR)}$ nt 3243G heteroplasmy on histone modifications; A. LC-MS/MS measurement of H4 acetylation from clustering experiment shows decreased H4 acetylation on all residues; **B.** Representative image of extracted histones Western blots reacted with antibodies to H4K5ac and H4 showing decreased H4K5 acetylation normalized to total histone 4; **C.** Quantification of western blots of H4K5ac/H4total (n = 6); **D.** Negative correlation of aKG levels with histone H3K9 trimethylation (**left**) and H3K9 dimethylation (**right**); Results shown as mean with SD error bars, * $p < 0.05$, ** $p < 0.01$, *** $p < 0.001$, **** $p < 0.0001$, ns – not significant, n = 3)

Supplementary Figure 4. Effect of mtDNA tRNA$^{Leu(UUR)}$ nt 3243G heteroplasmy on pyruvate metabolism, NADH accumulation, S-adenosylmethionine (SAM), and histone 4 acetylation; A. m.3243G-induced OXPHOS dysfunction shifts glucose metabolism away from acetyl-CoA and toward lactate production due to NADH accumulation; **B.** In an independent experiment, we quantified lactate production and intracellular acetyl-CoA across all 3243G cell lines (0% heteroplasmy indicated by green, 100% by read spots), revealing a strong inverse correlation between intracellular acetyl-CoA and lactate production (n = 3; t = 12 h); **C. Top left –** For each mole of glucose consumed, 100% mutant cells produce more lactate than 0% (wild type) counterparts (n = 3, t = 64 h, corrected for cell proliferation); **Top right** – intracellular acetyl-CoA concentration is reduced in 100% mutant cells compared to 0% (wild type) (n = 3); **bottom left** – NAD^+/NADH ratio measured by High Pressure Liquid Chromatography is lower in 100% mutant cells compared to 0% 3243G cells, n = 4; **Bottom right** – acetyl-CoA to free CoA ratio, acetyl-CoA is reduced in 100% mutant cells (n = 3); **D.** S-adenosyl-methionine concentration is decreased in 100% mutant cells; Results shown as mean with SD error bars, * $p < 0.05$, ** $p < 0.01$, ns – not significant, n = 3)

Supplementary Figure 5. Effect of mtDNA tRNA$^{Leu(UUR)}$ nt 3243G heteroplasmy, impaired mitochondrial protein synthesis and mitochondrial complex I inhibition on histone H4 acetylation; A. Steady-state levels of histone acetylation as fraction for each lysine of histone H4 for 0% and 100% 3243G cells and for 0% cells treated with CP and after CP washout; **B.** Proportion of acetylation on each histone H4 lysine derived from ^{13}C-labelled glucose for cell cultures as in A; **C.** Steady-state levels of histone acetylation as fraction for each lysine of histone H4 for 0% and 100% 3243G cells and for 0% cells after inhibition of complex I with rotenone; **D.** Steady-state levels of unmodified, monoacetylated (ac1), diacetylated (ac2), triacetylated (ac3) or tetraacetylated (ac4) histone H4 for cell cultures as in C; **E**. Proportion of acetylation on each histone H4 lysine derived from ^{13}C-labelled glucose for cell cultures as in C; **F**. Proportion of acetylation derived from ^{13}C-labelled glucose on mono and polyacetylated histone H4 for cell cultures as in C; **G.** Proportion of glutamine-derived acetylation on each histone H4 lysine for cell cultures as in C; **H.** Proportion of glutamine-derived acetylation on mono and polyacetylated histone H4 for cell cultures as in C; Results shown as mean with SD error bars, * $p < 0.05$, ** $p < 0.01$, *** $p < 0.001$, **** $p < 0.0001$, ns – not significant, A-B & E-H: n = 3, C-D: n = 6).

Supplementary Figure 6. Mitochondrial respiration of 0% 3243G cybrids cultured with and without CP; A. Representative trace showing oxygen consumption in 0% 3243G cells with and without inhibition of mitochondrial protein synthesis by CP; DGM – addition of digitonin (10ug/ml/2x10^6 cells) to permeabilize cell membrane, glutamate (final: 10 mM) and malate (2 mM) (complex I substrates); ADP – addition of ADP (2.5 mM) to assess ATP synthase coupled respiration; S – addition of succinate (10 mM) (complex II substrate) to measure OXPHOS oxygen consumption through both complexes I and II; O – addition of oligomycin (2.5 μM) to stop ATP synthase to measure proton leak rate; F – addition of FCCP (F2 – 2 μl, F1 1 μl of 1 mM stock) to uncouple the electron transport from the ATP synthase to determine maximal respiration; R – addition of rotenone (0.5 μM) to measure complex II-driven maximal respiration; A – addition of antimycin A (2.5 μM) to block electron flow through complex III to assess non-mitochondria oxygen consumption; **B.** Quantification of oxygen consumption: BASAL = respiration prior to addition of chemicals to the chamber, OXPHOS I versus OXPHOS II = respiration after addition of complex I or both complexes I and II substrates, respectively; relative to % 3243G mutant respiration, the presence of 100% 3243G mutation partially inhibits respiration while culture for seven days in 100 μg/ml CP results in complete inhibition of respiration, the effects of which are reversed by three days culture without CP; Results shown as mean with SD error bars, * $p < 0.05$, ** $p < 0.01$, *** $p < 0.001$, **** $p < 0.0001$, ns – not significant, n = 3)

Supplementary Figure 7. Histone acetylation changes due to m.3243A>G mutation are independent of glucose concentration in the media; A. Glucose concentration measurement after 4 h and 8 h incubation time of 0% (wild type) and 100% mutant cells shows that 4 h incubation of 100% cells and 8 h incubation of 0% cells result in the same glucose concentration in the media; **B.** Western blotting of H4K5 acetylation and total histone 3 (loading control) shows that 4 h 100% incubation and 8 h 0% incubation results in different H4K5ac level despite the same concentration of glucose in the media observed in **A; C.** Quantification of H4K5ac band intensity normalized to H3 total band intensity shows decreased acetylation of H4 at lysine 5 in spite of same concentration of glucose; media and histone extraction were carried out from the same plate for each experiment, results shown as mean with SD error bars, * $p < 0.05$, ** $p < 0.01$, *** $p < 0.001$, ns – not significant, $n = 3$)

Supplementary Figure 8. Graphic representation of the changes in mitochondrial metabolites, NAD^+/NADH ratio, histone modifications, and gene expression profiles observed in cybrid lines harboring increasing mtDNA $tRNA^{Leu(UUR)}$ nt 3243G heteroplasmy levels. The resulting associations suggest a model for the mitochondrial regulation of the nuclear epigenome.

Supplementary Figure 9. Quantification and stability of mtDNA $tRNA^{Leu(UUR)}$ nt 3243G heteroplasmy monitored using restriction fragment polymorphism PCR. A. Mixing of known quantities of 0% 3243G (wild type) and 100% 3243G mutant DNA confirms relative accuracy of the RFLP method. **B.** Heteroplasmy quantification at 3 different time points that encompass the total number of passages which the heteroplasmic cells have undergione during the duration of these experiments. The 143B(TK^-) cybrid cell lines maintained under our culture conditions sustain surprisingly stable hetetroplasmy levels.

Reference

1 Picard, M. *et al.* Progressive increase in mtDNA 3243A>G heteroplasmy causes abrupt transcriptional reprogramming. *Proc. Natl. Acad. Sci. USA* **111**, E4033-E4042, doi:10.1073/pnas.1414028111 (2014).

SUPPLEMENTARY FIGURE 1

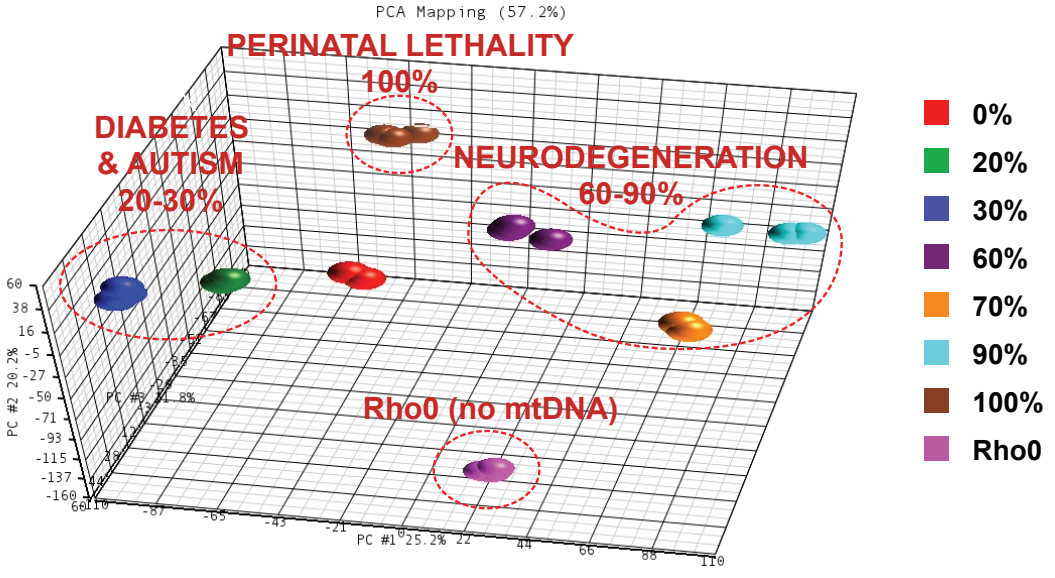

SUPPLEMENTARY FIGURE 2

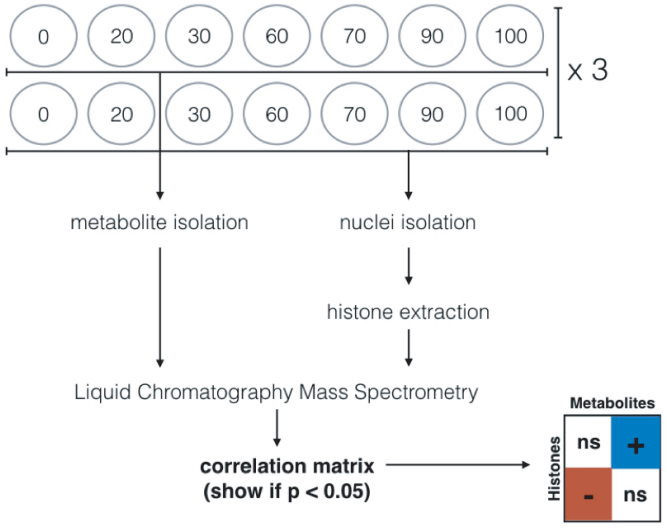

SUPPLEMENTARY FIGURE 3

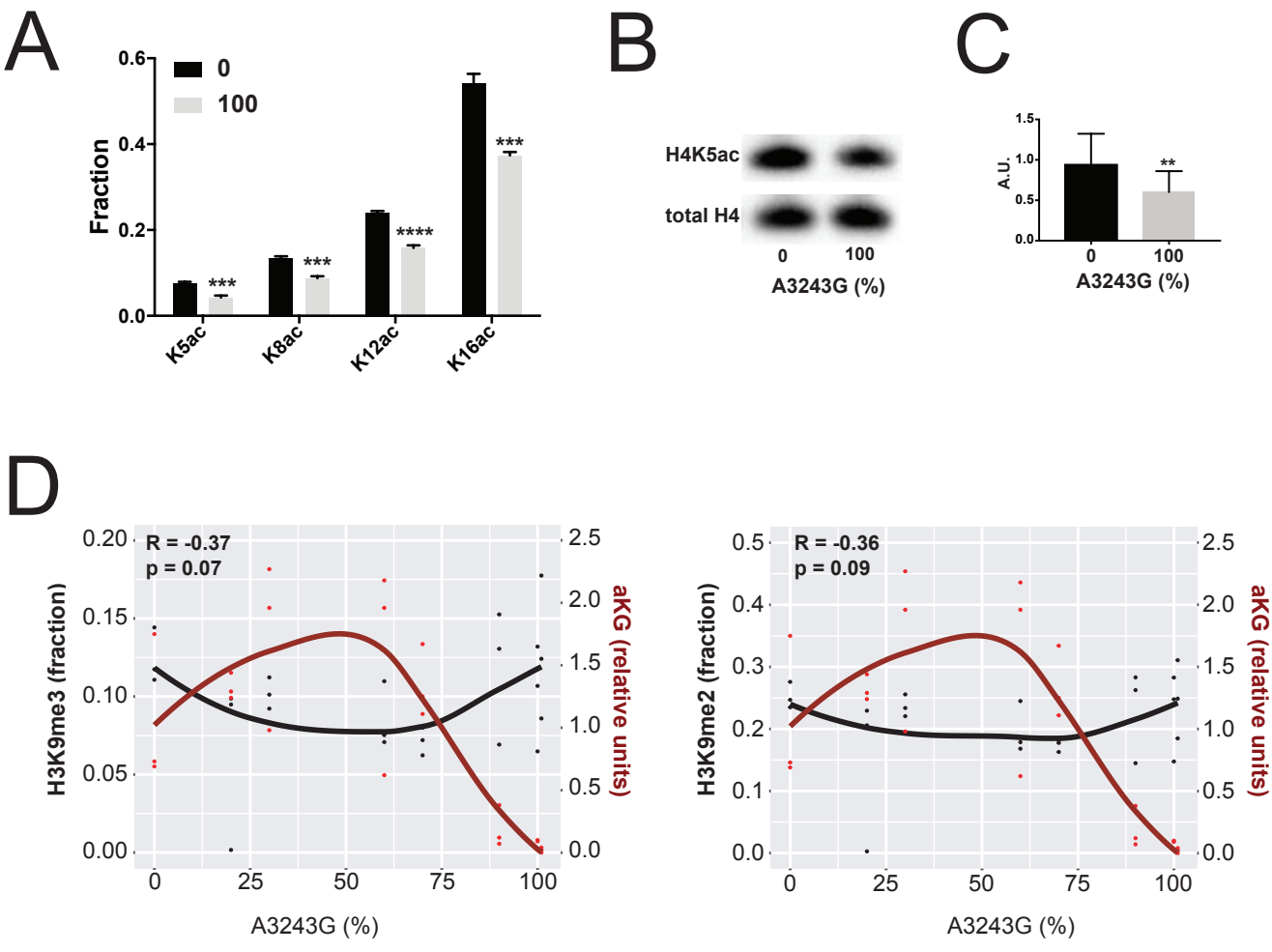

SUPPLEMENTARY FIGURE 4

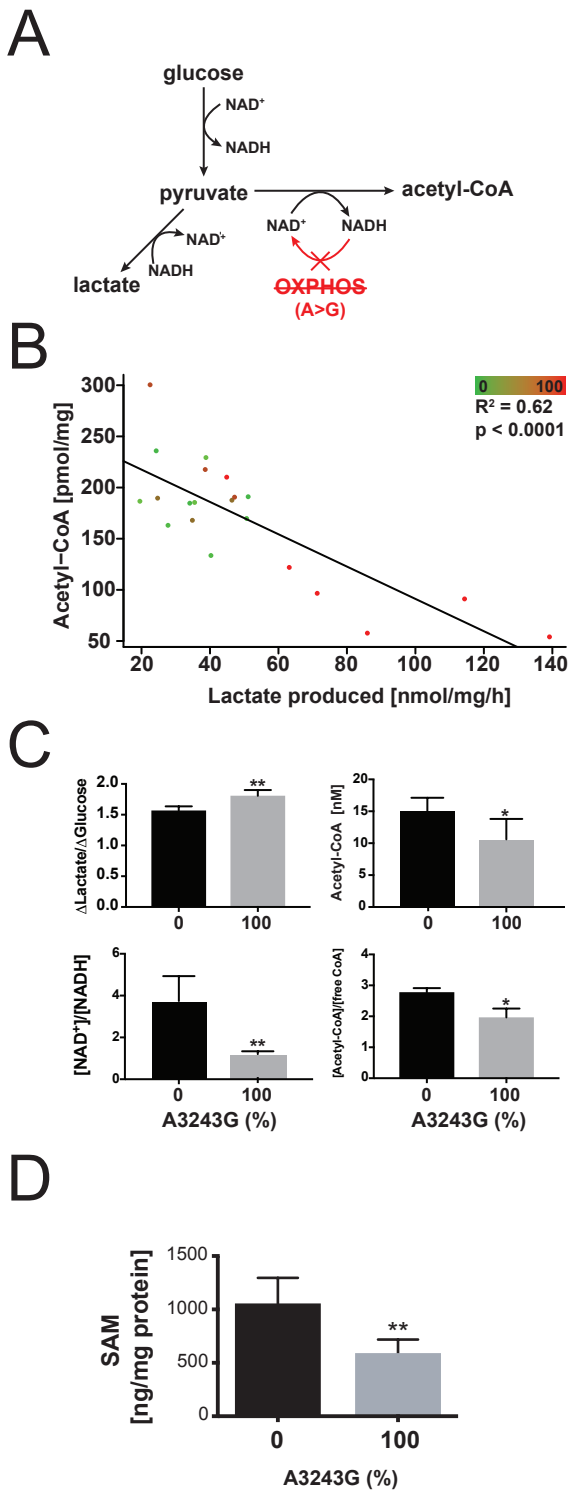

SUPPLEMENTARY FIGURE 5

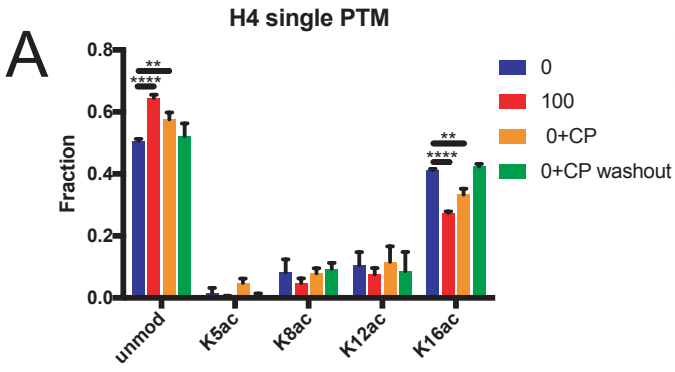

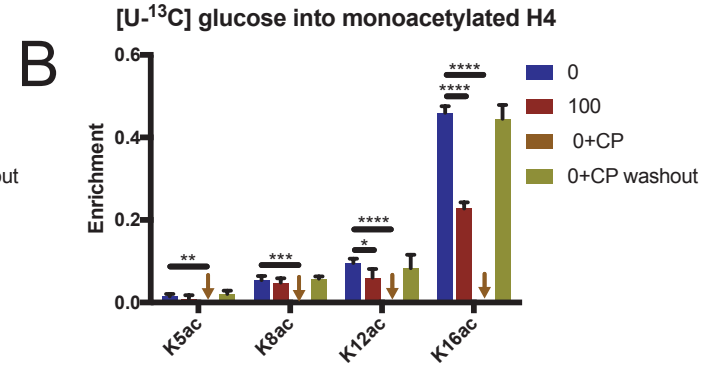

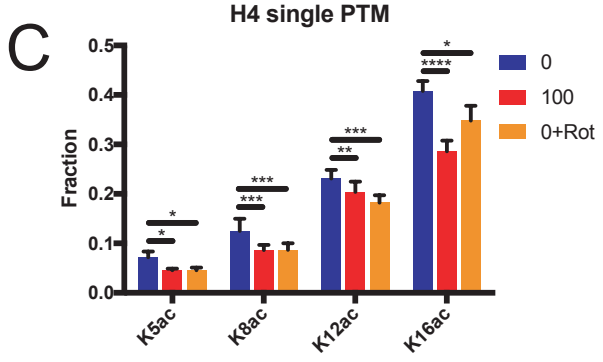

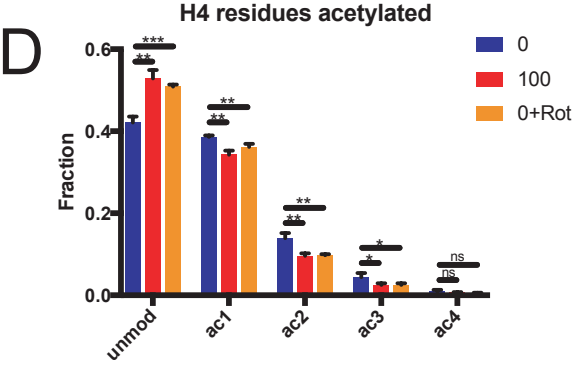

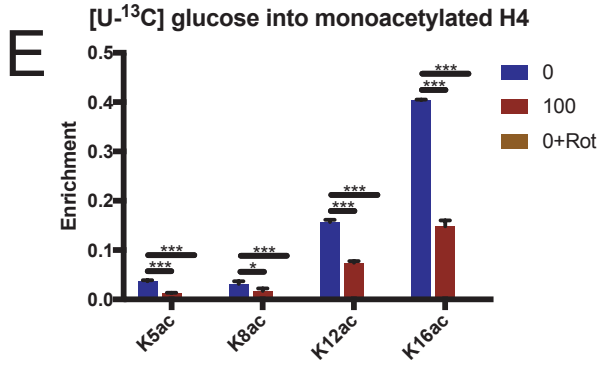

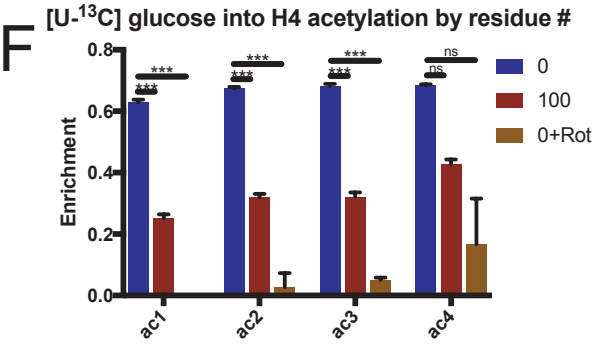

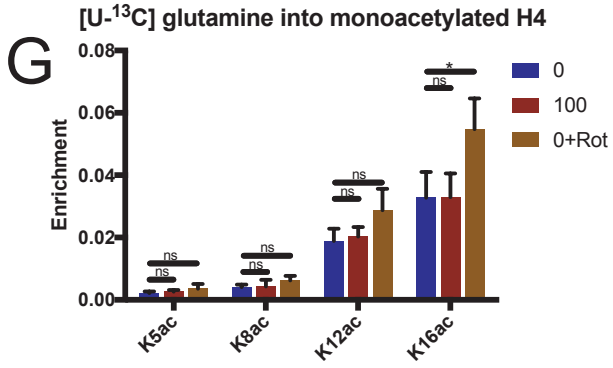

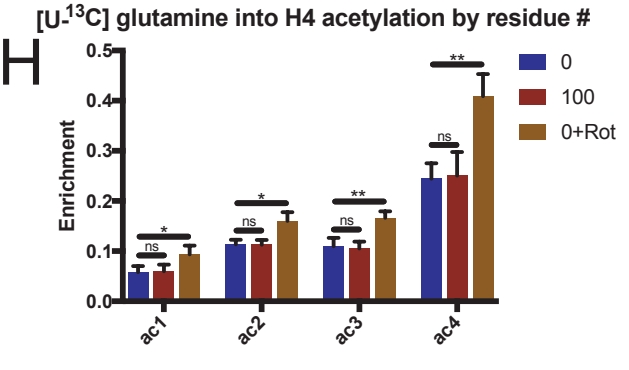

SUPPLEMENTARY FIGURE 6

A

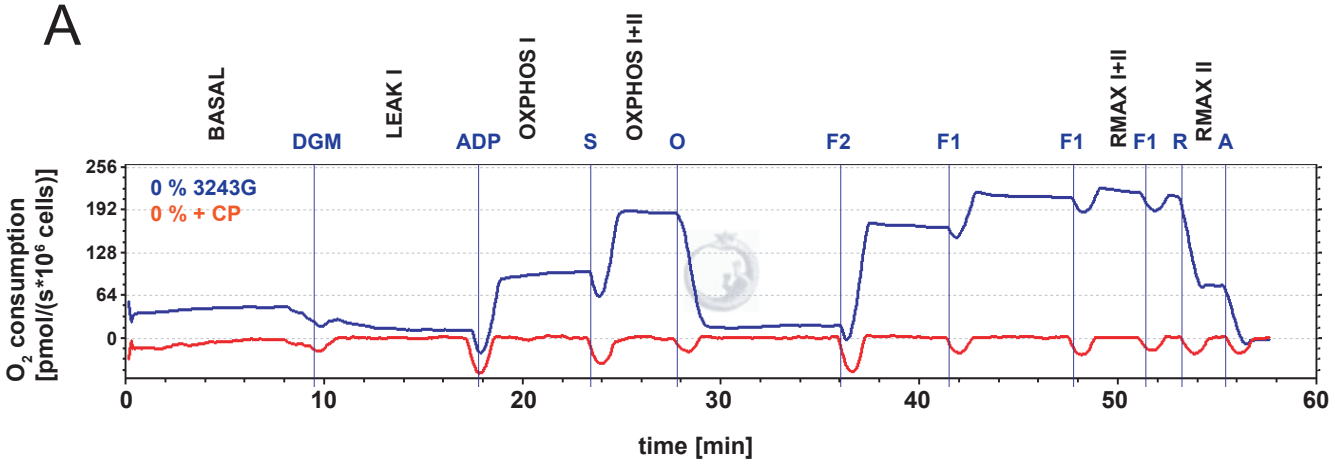

B

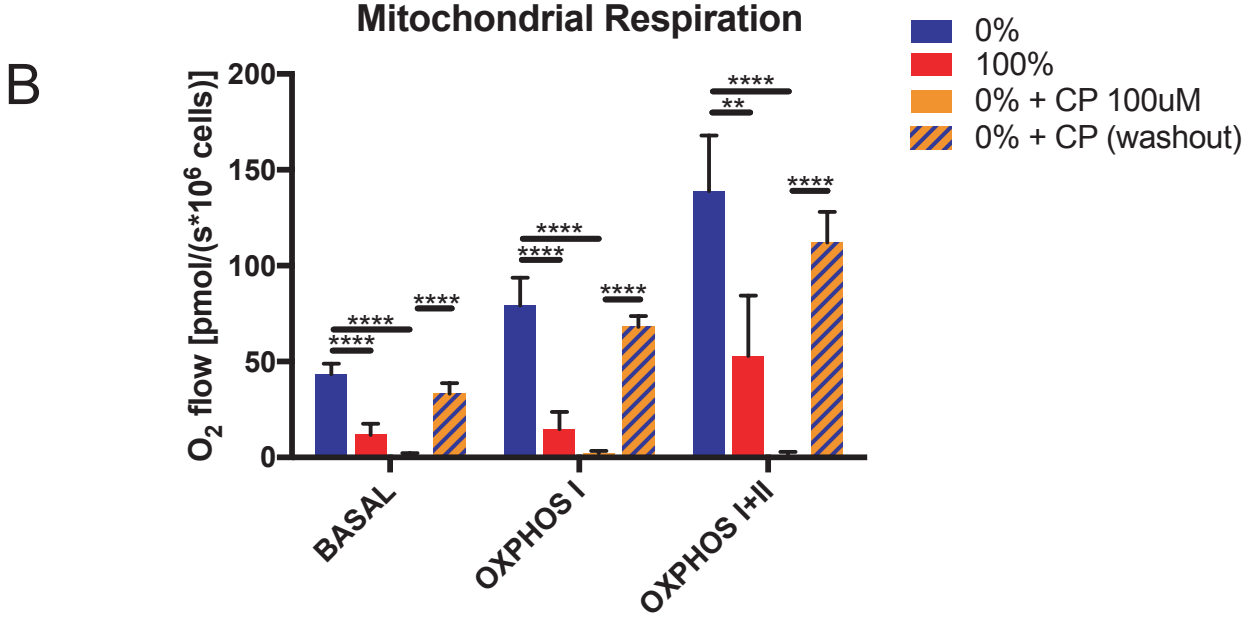

SUPPLEMENTARY FIGURE 7

A

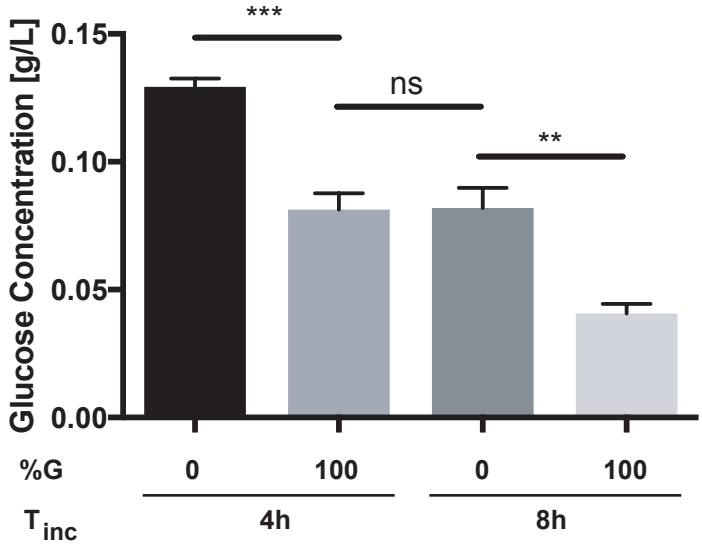

B

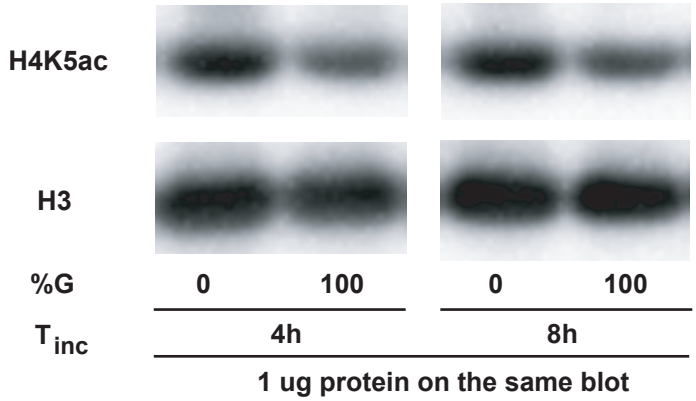

C

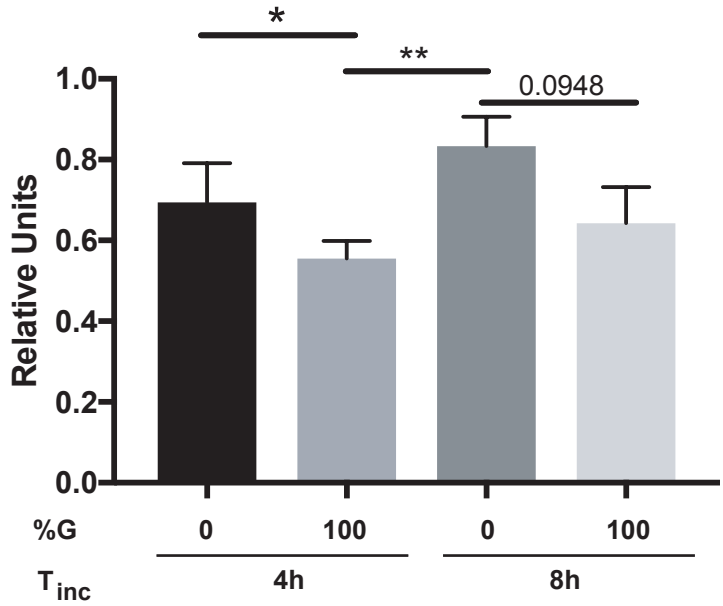

SUPPLEMENTARY FIGURE 8

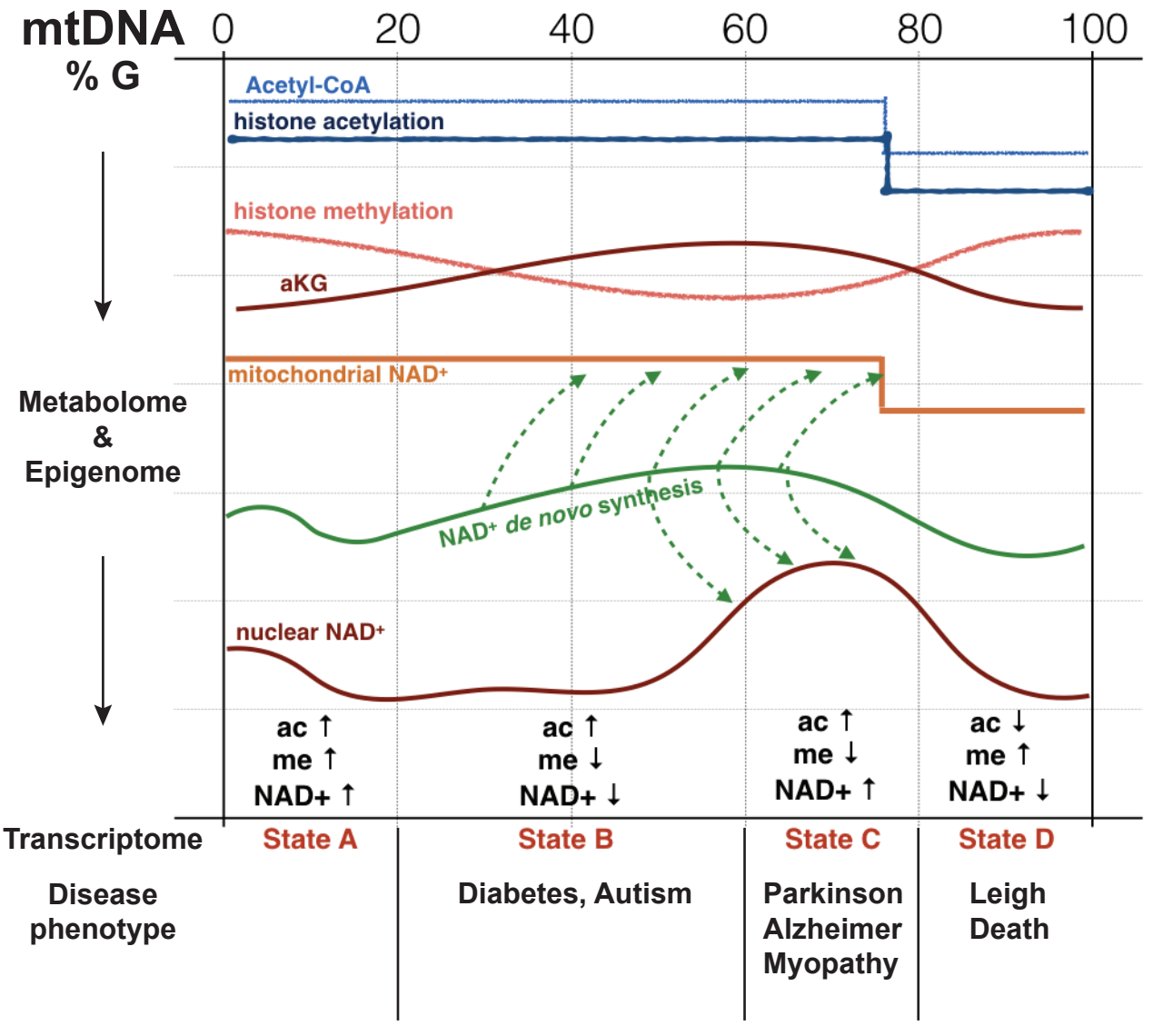

SUPPLEMENTARY FIGURE 9

A

Mixed %G	RFLP
0	0.31
10	10.34
20	20.04
30	29.44
40	38.99
50	48.74
60	60.01
70	68.99
80	75.28
90	87.70
100	99.69
no DNA	40.32

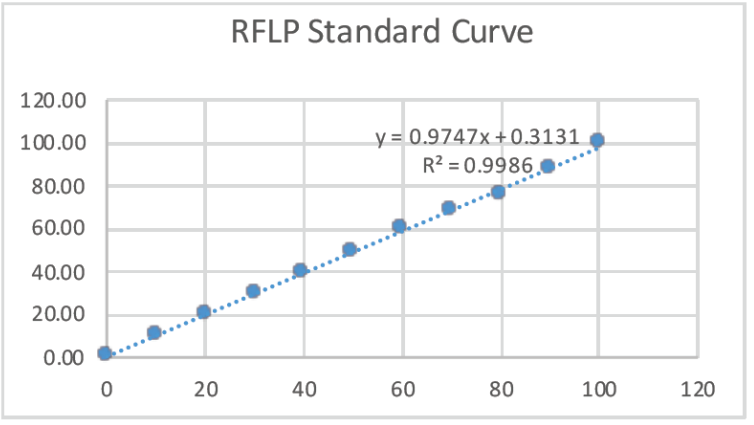

B

passage	n+3	n+4	n+5	average
CL9		0.00	0.43	0.21
DW4	16.15	17.55	17.62	17.11
DW5	36.37	33.64	35.89	35.30
DW9	61.60	62.42	60.65	61.56
DW7	69.35	71.69	72.13	71.05
DW10	97.72	98.06		97.89
CL3		100.00	100.00	100.00